ChemComm

COMMUNICATION

View Article Online
View Journal | View Issue

Cite this: *Chem. Commun.*, 2020, **56**, 9970

Received 4th May 2020,
Accepted 23rd July 2020

DOI: 10.1039/d0cc03215h

rsc.li/chemcomm

Reduction of carbon dioxide at a plasmonically active copper–silver cathode†

Elizabeth R. Corson,[ab] Ananya Subramani,[ab] Jason K. Cooper,[b] Robert Kostecki,[bc] Jeffrey J. Urban[bd] and Bryan D. McCloskey *[abc]

Electrochemically deposited copper nanostructures were coated with silver to create a plasmonically active cathode for carbon dioxide (CO_2) reduction. Illumination with 365 nm light, close to the peak plasmon resonance of silver, selectively enhanced 5 of the 14 typically observed copper CO_2 reduction products while simultaneously suppressing hydrogen evolution. At low overpotentials, carbon monoxide was promoted in the light and at high overpotentials ethylene, methane, formate, and allyl alcohol were enhanced upon illumination; generally C_1 products and C_2/C_3 products containing a double carbon bond were selectively promoted under illumination. Temperature-dependent product analysis in the dark showed that local heating is not the cause of these selectivity changes. While the exact plasmonic mechanism is still unknown, these results demonstrate the potential for enhancing CO_2 reduction selectivity at copper electrodes using plasmonics.

Carbon dioxide (CO_2) reduction can prevent emission of CO_2 into the atmosphere while simultaneously generating valuable products to be used as renewable fuels and chemical precursors. The key challenge in CO_2 reduction is selectively producing multiple-carbon-containing compounds that have higher energy density or higher value than single carbon (C_1) products like methane or carbon monoxide (CO). Copper (Cu) catalysts are well known for their ability to form many two- and three-carbon products (C_2 and C_3), but these products are formed concurrently and often with low faradaic efficiencies (FE).[1]

Recently we have explored the use of localized surface plasmon resonance (LSPR) in roughened or nanostructured silver (Ag) electrodes to address poor CO_2 reduction selectivity.[2,3] Nanostructured plasmonic metals exhibit peak plasmon resonance at a specific wavelength of light that can be tuned by changing the size, shape, and composition of the nanostructures.[4] The LSPR can decay to form energetic electron–hole pairs and can generate strong local electric fields, both of which can interact with adsorbates at the cathode surface and influence electrochemical reactions.[4,5] We have shown that an illuminated, plasmonically active Ag cathode enhances all CO_2 reduction products, increasing the formation of CO, formate, and methanol while simultaneously suppressing undesired hydrogen (H_2) evolution.[2,3] Here we investigate a plasmonically active Cu–Ag cathode, combing nanostructured Cu, that has catalytic activity for multi-carbon-containing CO_2 reduction products, with highly plasmonic Ag in an effort to create a more selective catalyst. We explore the changes in product distribution in the light and the dark and with temperature in a custom temperature-controlled photoelectrochemical cell[6] to determine if the plasmonic activity of Ag combined with the catalytic properties of Cu can direct CO_2 reduction towards the formation of select valuable products.

Cu nanocorals were electrochemically formed on the surface of a Ag foil following the procedure reported by Gurudayal *et al.*, where a high current density results in the formation of H_2 bubbles that define the nanofeature morphology.[7,8] We selected the nanocoral morphology to study here given their sharp features that should serve to enhance the LSPR (Fig. 1B). Despite the bare Cu nanocorals having high optical absorbance across the visible spectrum (Fig. S1, ESI†), the photocurrent density was small (Fig. S4C, ESI†). To enhance the plasmonic photocurrent, 10 nm of Ag was deposited by electron-beam (e-beam) evaporation, forming the "cathode" (Fig. S5, ESI†). This was expected to improve the cathodic photocurrent because Ag has been theoretically shown to produce a bimodal distribution of high-energy electrons and holes, whereas Cu photoexcitation results in a hole-dominant energy distribution.[9] Scanning electron microscopy (SEM) images show a heterogeneous coverage of Cu

[a] *Department of Chemical and Biomolecular Engineering, University of California, Berkeley, California 94720, USA. E-mail: bmcclosk@berkeley.edu*
[b] *Joint Center for Artificial Photosynthesis, Lawrence Berkeley National Laboratory, Berkeley, California 94720, USA*
[c] *Energy Storage and Distributed Resources Division, Lawrence Berkeley National Laboratory, Berkeley, California 94720, USA*
[d] *The Molecular Foundry, Lawrence Berkeley National Laboratory, Berkeley, California 94720, USA*

† Electronic supplementary information (ESI) available: Cathode fabrication and characterization through SEM, EDS, XPS, XRD, and UV-vis; electrochemical techniques; photocurrent measurements; product analysis through GC and NMR. See DOI: 10.1039/d0cc03215h

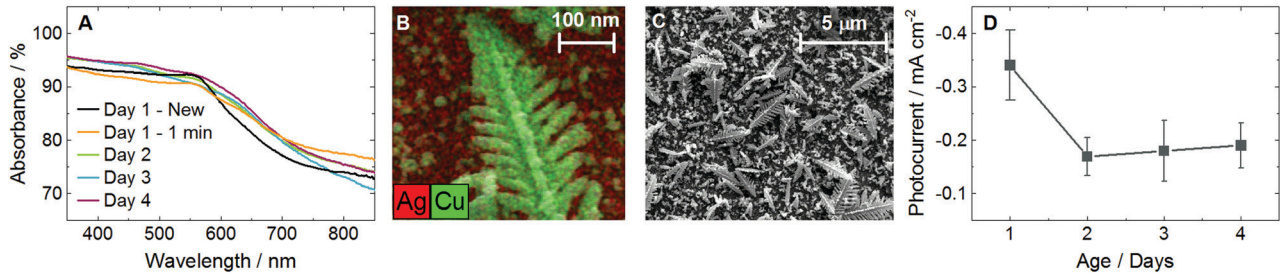

Fig. 1 Characterization of the cathode stability. (A) UV-visible (UV-vis) absorbance of plasmonically active cathodes as-prepared, after 1 minute of chronoamperometry (CA) at −1.0 V_{RHE}, and after 2, 3, and 4 days of electrochemical experiments. Different cathodes were measured for each day. (B) Energy-dispersive X-ray spectroscopy (EDS) of a nanocoral feature on the surface of the cathode after 3 days of electrochemical experiments. (C) Scanning electron microscopy (SEM) of the cathode surface after 4 days of electrochemical experiments. (D) Photocurrent over time during CA at −0.78 V_{RHE} with 365 nm LED illumination at 170 mW cm^{-2}. Error bars represent one standard deviation of experiments performed in triplicate. See Fig. S1–S3 for further UV-vis plots, Fig. S4 for more photocurrent plots, and Fig. S6 and S7 for additional SEM and EDS images (ESI†).

features ranging from 10 nm to 2 μm in size with no apparent change observed by SEM in the Cu features after 1 to 4 days of electrochemical experiments (Fig. 1C and Fig. S6, ESI†). The energy-dispersive X-ray spectroscopy (EDS) image in Fig. 1B shows the dominant Cu composition of the nanocorals and the tilted EDS image in Fig. S7E (ESI†) more clearly shows the 10 nm Ag layer. X-ray diffraction (XRD) indicates that both Ag and Cu are polycrystalline (Fig. S8, ESI†). X-ray photoelectron spectroscopy (XPS) shows a decrease in the ratio of Ag to Cu after 180 minutes of chronoamperometry (CA) at −1.0 V_{RHE} (*V vs.* the reversible hydrogen electrode) (Fig. S9, ESI†).

The absorbance measured by UV-visible spectroscopy (UV-vis) showed a flattening of the observable plasmonic peak at 560 nm after just 1 minute of CA at −1.0 V_{RHE}, but thereafter remained relatively constant over 4 days of electrolysis (Fig. 1A and Fig. S2, ESI†). While the peak at 560 nm matches the plasmon resonance of Cu, it was found that photocurrent measurements were maximized under 365 nm illumination, close to the plasmon resonance of Ag (Fig. S3, ESI†). Fig. S4D (ESI†) shows that the decreasing photocurrent density from 365 to 525 nm followed the absorbance trend measured by UV-vis, but where the absorbance only dropped by 2% in this range the photocurrent was diminished by 90%. Thus, all experiments in this study performed in the "light" were conducted with a 365 nm light-emitting diode (LED) at 170 mW cm^{-2}. The peak photocurrent of a new cathode, −0.34 mA cm^{-2}, decreased after exposure to electrolysis but stabilized over 4 days of use at −0.18 mA cm^{-2}, nearly twice the peak photocurrent of bare Cu nanocorals, −0.10 mA cm^{-2} (Fig. 1D and Fig. S4C, ESI†). We observed that the gaseous product distribution at −0.8 V_{RHE} in the dark and the light was constant over 3 days of electrolysis (Fig. S10, ESI†). From the XPS, photocurrent, UV-vis, and product distribution trends over time we conclude that the e-beam deposited Ag does initially reorganize during electrolysis but stabilizes in a structure that is distinct from, and more plasmonically active than, bare Cu nanocorals.

The product distribution was investigated from −0.6 to −1.0 V_{RHE} under dark and light conditions at 22 °C in 0.1 M potassium bicarbonate ($KHCO_3$) continuously sparged by CO_2. 15 products were detected, but only 5 were selectively enhanced upon illumination. The FE of majority species (>1%) is shown in Fig. 2 with the corresponding partial current densities shown in Fig. S11 (ESI†). The FE and partial current densities of minority species can be found in Fig. S12 and S13 (ESI†). All detected products are listed in Table S1 (ESI†). Of the 14 products reported by Gurudayal *et al.* on bare Cu nanocorals,[7] only ethylene glycol was not detected in this study. We measured two additional products, gycolaldehyde and acetone, which have previously been reported as CO_2 reduction products

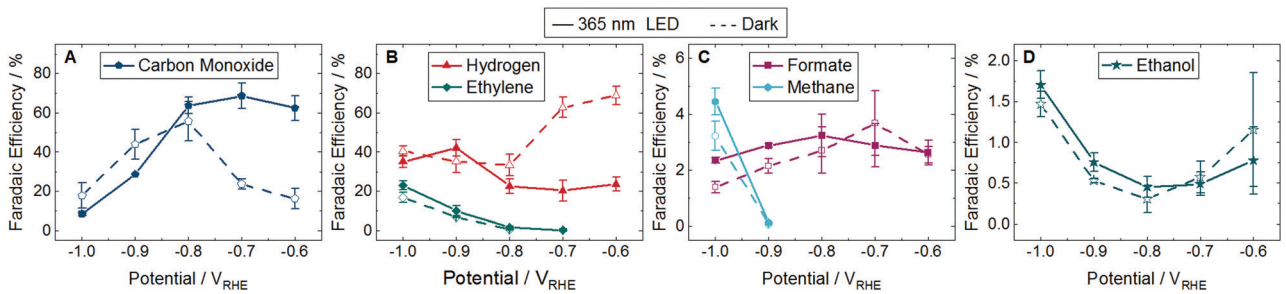

Fig. 2 Faradaic efficiency (FE) of major products from −0.6 to −1.0 V_{RHE} at 22 °C. Dashed lines with unfilled symbols show results performed in the dark and solid lines with filled symbols show results performed under continuous illumination using a 365 nm LED with an intensity of 170 mW cm^{-2}. No points are plotted if the product was not detected. Products shown are (A) carbon monoxide, (B) hydrogen and ethylene, (C) formate and methane, and (D) ethanol. Fig. S11 in the ESI† shows the partial current densities for these major products. The FE and partial current densities of the minority products methanol, glycolaldehyde, acetaldehyde, ethane, hydroxyacetone, acetone, allyl alcohol, propionaldehyde, and *n*-propanol are shown in Fig. S12 and S13 in the ESI,† respectively. Error bars represent one standard deviation of experiments performed in triplicate.

on Cu foil.[1] While there are variations in the dark product distribution between our study and that of Gurudayal *et al.*,[7] the most notable difference is an increase in CO production, as expected from the addition of Ag.

At low overpotentials (−0.6 and −0.7 V_{RHE}) CO production was enhanced in the light and H_2 was suppressed. While there was no difference in H_2 production in the dark and light at high overpotentials (−0.8, −0.9, and −1.0 V_{RHE}), a suppression of CO FE and partial current density was observed in the light at −0.9 and −1.0 V_{RHE}. At these same potentials we find an enhancement of ethylene, methane, formate, and allyl alcohol. These CO, H_2, and formate trends in the light are similar to those reported on a plasmonically active Ag cathode.[3] However, where Creel *et al.*[3] found that all CO_2 reduction products were enhanced in the light, we find that the illuminated Cu–Ag cathode is only selective to 5 of the 14 CO_2 reduction products.

CO is widely cited as an intermediate in the reaction pathway to ethylene and methane.[10] While the exact reaction pathways of C_3 products are unknown,[1] it has been shown that CO can be reduced to propionaldehyde, *n*-propanol, and allyl alcohol.[11,12] This consumption of CO to create further reduced products may account for the decrease in CO production in the light at these high overpotentials.

While 4 of the 5 major CO_2 reduction species were influenced by the light, ethanol showed no difference between the light and the dark at any applied potential (Fig. 2D and Fig. S11D, ESI†). Many of the minority products were only produced at potentials cathodic to −1.0 V_{RHE} and all but allyl alcohol have overlapping error bars, indicating no distinction between the light and the dark (Fig. S12 and S13, ESI†). Of the minority products, only methanol was detected at every applied potential investigated. There was no difference between methanol results in the light and the dark, and the FE remained below 0.15%. This is in contrast to the results on a plasmonically active Ag cathode, where methanol was only formed in the light at up to 2% FE.[3]

Chemical groupings reveal some trends in the selectivity of CO_2 reduction products. C_1 products (CO, formate, and methane) are generally enhanced in the light, with the exception of methanol. Of C_2 products, only ethylene production is promoted in the light while no significant change is observed in ethanol, glycolaldehyde, acetaldehyde, or ethane. Of C_3 products, only allyl alcohol showed a significant increase in the light, with no difference measured between the light and the dark for propionaldehyde, acetone, *n*-propanol, or hydroxyacetone.

We also look for trends by functional groups. Alkanes show mixed results with methane enhanced in the light but no change for ethane. The only alkene, ethylene, is promoted in the light. The primary alcohols—methanol, ethanol, and *n*-propanol—showed no difference between light and dark, but allyl alcohol, which has a double carbon bond like ethylene, was enhanced in the light. No aldehydes were influenced by the light (glycolaldehyde, acetaldehyde, and propionaldehyde). Finally, ketones experienced no difference between the light and the dark, namely acetone and hydroxyacetone, which also have a hydroxyl functional group like the alcohols.

It is possible for plasmons to decay into phonons, resulting in localized heating that can influence product selectivity.[5] To determine if localized heating was a contributing factor, we measured the product distribution at −0.6 and −1.0 V_{RHE} in the dark at 14, 22, and 35 °C in otherwise identical conditions. The FE of majority species are shown in Fig. 3 with the corresponding partial current densities shown in Fig. S14 (ESI†). The FE and partial current densities of minority species can be found in Fig. S15 and S16 (ESI†). At −0.6 V_{RHE} CO production in dark conditions showed no trends with temperature (Fig. 3A), as opposed to the increase in CO FE in the light (Fig. 2A). H_2 formation at −0.6 V_{RHE} increased with increasing temperature (Fig. 3B), opposite of the decrease in H_2 production observed in the light (Fig. 2B). At −1.0 V_{RHE} CO production increased with increasing temperature (Fig. 3A), in direct contrast with the decrease in CO observed in the light (Fig. 2A). Similarly, the production of ethylene, methane, formate, and allyl alcohol decreased with increasing temperature at −1.0 V_{RHE} (Fig. 3B, C, and Fig. S15G, ESI†), the opposite trend observed in the light (Fig. 2B, C, and Fig. S12G, ESI†). Because the product distribution changes caused by the light do not match the product selectivity at elevated temperatures, we conclude that localized heating from plasmon decay

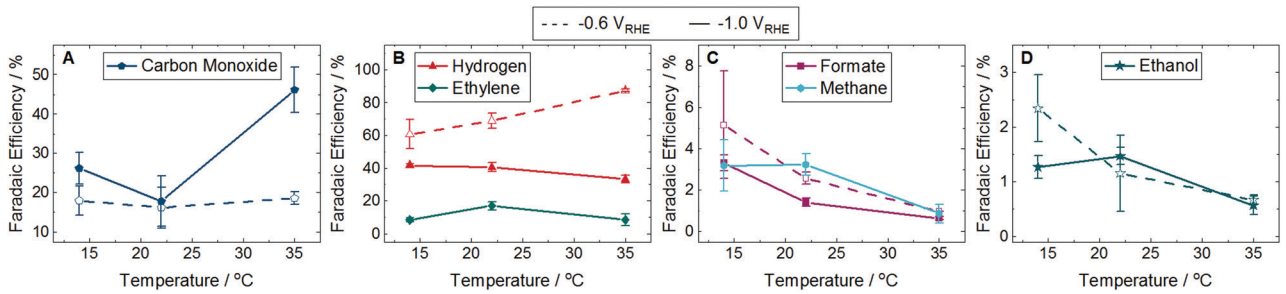

Fig. 3 Faradaic efficiency (FE) of major products at 14, 22, and 35 °C in the dark. Dashed lines with unfilled symbols show results performed at −0.6 V_{RHE} and solid lines with filled symbols show results performed at −1.0 V_{RHE}. Products shown are (A) carbon monoxide, (B) hydrogen and ethylene, (C) formate and methane, and (D) ethanol. Fig. S14 in the ESI† shows the partial current densities for these major products. Ethylene and methane were not detected at any temperature at −0.6 V_{RHE}. The FE and partial current densities of the minority products methanol, glycolaldehyde, acetaldehyde, ethane, hydroxyacetone, acetone, allyl alcohol, propionaldehyde, and *n*-propanol are shown in Fig. S15 and S16 in the ESI,† respectively. Error bars represent one standard deviation of experiments performed in triplicate.

is not contributing to the enhancement of CO_2 reduction in the light.

In addition, we measured the photocurrent at different intensities of 365 nm LED illumination while applying -0.78 V_{RHE} during normal CO_2 reduction conditions (Fig. S4E, ESI†). The photocurrent increased linearly with increasing light intensity which, because we would expect an exponential dependence in the case of heating, further demonstrates an athermal plasmonic mechanism.[13]

Other possible plasmonic mechanisms include a permanent or temporary hot electron transfer to an unoccupied molecular orbital (MO) of an adsorbate, or an enhancement of the local electric field (Fig. S18, ESI†).[4,5] In prior work using *in situ* infrared spectroscopy at a plasmonically active Ag cathode we showed that the increase in CO production at low overpotentials was likely due to an enhanced desorption of CO in the light.[14] This can be understood through a desorption induced by electronic transitions (DIET) mechanism, where an excited metal–CO complex gains enough energy to overcome the activation barrier for desorption before the hot electron decays back to the metal.[4] Because the CO selectivity trends in the light are very similar on this Cu–Ag cathode, it is possible that this DIET mechanism also explains the enhanced CO production in the light at -0.6 and -0.7 V_{RHE}. In the same study we found that light increased the bond strength of bicarbonate (HCO_3^-) at the surface, likely as a result of the enhanced local electric field.[14] This would cause an increase in the local pH, depleting the concentration of protons at the surface and thus suppressing H_2 evolution.[15] Again, because H_2 evolution is also suppressed in the light on this Cu–Ag cathode, the same local electric field mechanism may account for this behavior. However, there is not enough experimental evidence at this time to conclusively determine the plasmonic mechanism influencing CO or H_2 selectivity.

This additional increase in the local pH in the light may explain the results observed at low overpotentials, but it cannot account for the behavior at high overpotentials. Hori *et al.* showed that in higher pH environments methane formation is suppressed and ethylene production is enhanced.[16] However, we find that both ethylene and methane are enhanced in the light at -1.0 V_{RHE}. Because formate, methane, and ethylene represent branching pathways in the CO_2 reduction reaction, it is likewise difficult to pinpoint a common reaction intermediate that may be selectively accepting a hot electron.[10,16]

In conclusion, we combined nanostructured Cu with Ag to create a plasmonically active cathode that was stable over multiple days of use. Where a Ag cathode enhanced all CO_2 reduction products in the light,[3] this Cu–Ag cathode is selective to 5 of 14 CO_2 reduction products upon illumination while simultaneously suppressing H_2 evolution, compared to similar results in the dark. At higher overpotentials this Cu–Ag catalyst enhances ethylene, methane, formate, and allyl alcohol in the light; generally C_1 products and C_2/C_3 species with a double carbon bond. A temperature-dependent study showed that product selectivity trends at elevated temperatures are exactly opposite of the behavior we observe upon illumination. In addition, the photocurrent was found to increase linearly with increasing light intensity. From these results we can conclusively state that local heating is not the cause of the selectivity changes in the light, although the exact plasmonic mechanism is still unknown.

This enhancement of select CO_2 reduction products on Cu is a promising demonstration of the potential for plasmon-enhanced electrochemical conversion. With more investigation into the plasmonic mechanisms that influence product selectivity, we can begin to tune plasmonic properties through nanostructure size, shape, and composition to develop a highly selective, plasmonically active catalyst for CO_2 reduction.

This work was supported by the National Science Foundation (NSF), Grant No. CBET-1653430. Work was performed at the Joint Center for Artificial Photosynthesis, a DOE Energy Innovation Hub, supported through the Office of Science of the U.S. Department of Energy, Award No. DE-SC0004993. Work at the Molecular Foundry was supported by the Office of Science, Office of Basic Energy Sciences of the U.S. Department of Energy, Contract No. DE-AC02-05CH11231. E. R. C. received support from the NSF Graduate Research Fellowship, Grant No. DGE 1106400.

Conflicts of interest

There are no conflicts to declare.

References

1 K. P. Kuhl, E. R. Cave, D. N. Abram and T. F. Jaramillo, *Energy Environ. Sci.*, 2012, **5**, 7050–7059.
2 Y. Kim, E. B. Creel, E. R. Corson, B. D. McCloskey, J. J. Urban and R. Kostecki, *Adv. Energy Mater.*, 2018, **8**, 1800363.
3 E. B. Creel, E. R. Corson, J. Eichhorn, R. Kostecki, J. J. Urban and B. D. McCloskey, *ACS Energy Lett.*, 2019, **4**, 1098–1105.
4 S. Linic, P. Christopher and D. B. Ingram, *Nat. Mater.*, 2011, **10**, 911–921.
5 S. Linic, U. Aslam, C. Boerigter and M. Morabito, *Nat. Mater.*, 2015, **14**, 567–576.
6 E. R. Corson, E. B. Creel, Y. Kim, J. J. Urban, R. Kostecki and B. D. McCloskey, *Rev. Sci. Instrum.*, 2018, **89**, 055112.
7 Gurudayal, J. Bullock, D. F. Srankó, C. M. Towle, Y. Lum, M. Hettick, M. C. Scott, A. Javey and J. Ager, *Energy Environ. Sci.*, 2017, **10**, 2222–2230.
8 Gurudayal, J. W. Beeman, J. Bullock, H. Wang, J. Eichhorn, C. Towle, A. Javey, F. M. Toma, N. Mathews and J. W. Ager, *Energy Environ. Sci.*, 2019, **12**, 1068–1077.
9 R. Sundararaman, P. Narang, A. S. Jermyn, W. A. Goddard and H. A. Atwater, *Nat. Commun.*, 2014, **5**, 5788.
10 R. Kortlever, J. Shen, K. J. Schouten, F. Calle-Vallejo and M. T. M. Koper, *J. Phys. Chem. Lett.*, 2015, **6**, 4073–4082.
11 Y. Hori, R. Takahashi, Y. Yoshinami and A. Murata, *J. Phys. Chem. B*, 1997, **101**, 7075–7081.
12 E. Perez-Gallent, G. Marcandalli, M. C. Figueiredo, F. Calle-Vallejo and M. T. M. Koper, *J. Am. Chem. Soc.*, 2017, **139**, 16412–16419.
13 S. Mukherjee, L. Zhou, A. M. Goodman, N. Large, C. Ayala-Orozco, Y. Zhang, P. Nordlander and N. J. Halas, *J. Am. Chem. Soc.*, 2014, **136**, 64–67.
14 E. R. Corson, R. Kas, R. Kostecki, J. J. Urban, W. A. Smith, B. D. McCloskey and R. Kortlever, *J. Am. Chem. Soc.*, 2020, **142**, 11750–11762.
15 Y. Yoon, A. S. Hall and Y. Surendranath, *Angew. Chem., Int. Ed.*, 2016, **55**, 15282–15286.
16 Y. Hori, A. Murata and R. Takahashi, *J. Chem. Soc.*, 1989, 2309–2326.